(19) Europäisches Patentamt
European Patent Office
Office européen des brevets

(11) Publication number: **0 241 812**
A2

(12) EUROPEAN PATENT APPLICATION

(21) Application number: **87104872.4**

(51) Int. Cl.4: **C22C 37/04**

(22) Date of filing: **02.04.87**

(30) Priority: **07.04.86 US 848612**

(43) Date of publication of application:
21.10.87 Bulletin 87/43

(84) Designated Contracting States:
CH DE FR GB IT LI

(71) Applicant: **GENERAL ELECTRIC COMPANY**
1 River Road
Schenectady New York 12305(US)

(72) Inventor: **Farrell, Thomas Raymond**
26 Fredericks Road
Scotia, New York, 12302(US)

(74) Representative: **Catherine, Alain et al**
General Electric - Deutschland Munich
Patent Operation Frauenstrasse 32
D-8000 München 5(DE)

(54) Ferritic ductile iron for elevated temperature applications.

(57) Elevated temperature brittleness may be avoided in ferritic ductile iron by limiting the presence of residual quantities of sulfur (S) and residual quantities of magnesium (Mg) by percent by weight such that the parameter (Mg + 4.5S) is no greater than 0.070.

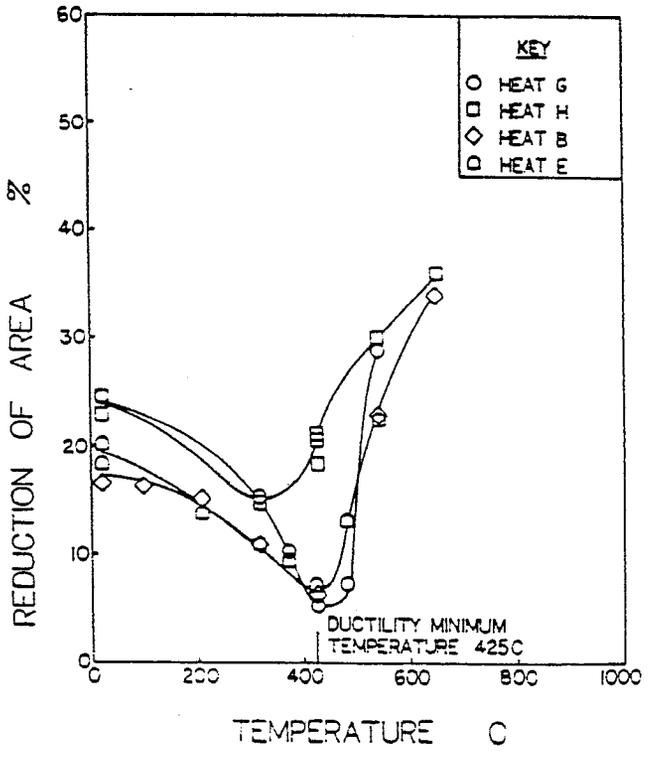

Figure 1. Tensile Area Reduction of Heats B, E, G and H as a Function of Temperature

EP 0 241 812 A2

FERRITIC DUCTILE IRON FOR ELEVATED TEMPERATURE APPLICATIONS

BACKGROUND OF THE INVENTION

Field of the Invention

This invention relates generally to a ferritic iron composition having improved elevated temperature properties, and particularly relates to a ferritic ductile iron composition which is substantially immune to elevated temperature brittleness.

Description of Prior Developments

Ferritic ductile iron is an important engineering alloy having several advantages over steel products, including low material cost and castability. However, for elevated temperature applications, steel products tend to be chosen for their superior mechanical properties. The phenomenon of elevated temperature brittleness (ETB) is in part responsible for the inability of ductile iron to compete with steels in such applications. This is particularly true in cases where good thermal fatigue resistance is required such as turbine casing applications, high pressure vessels and engine components.

Although the phenomenon of brittleness of ferritic ductile iron at elevated temperatures has been known for many years, little has been done to understand it. It has been shown that ETB manifests itself within a fairly narrow elevated temperature region by its pronounced effect on various physical properties. Such effects include reduced tensile strength, reduced tensile ductility and reduced low cycle fatigue resistance. The cause of these adverse effects on such material properties has been found to be the direct result of intergranular fracture.

It has also been determined that the temperature at which ductility is minimized is variable and is strain rate dependent. For the iron in question, this temperature occurs at 400C (725F) and 500C (932F) for strain rates of 2.8×10^{-4} sec $^{-1}$ and 1.4×10^{-2}, respectively. However, even with this knowledge, a solution to the problem of ETB has heretofore eluded the foundry industry.

Accordingly, a need exists for a ferritic ductile iron which exhibits improved elevated temperature properties including improved tensile ductility, improved low cycle thermal fatigue capability and reduced intergranular fracture.

SUMMARY OF THE INVENTION

The present invention has been developed to overcome the temperature related drawbacks of conventional iron by providing a new ferritic ductile iron having improved strength, ductility and thermal fatigue resistance at elevated temperatures. Extensive testing of the effects of chemical composition, strain rate and temperature have led to the discovery that certain ductile iron compositions may be produced which are substantially immune to ETB and which exhibit improved fatigue properties comparable to several common steels.

The characteristics of ETB have been found to be similar to metal induced embrittlement in that both phenomena exhibit onset and recovery and a strain rate effect. Reduced mechanical properties associated with ETB have been found to be the direct result of the development of intergranular fracture which develops upon reaching maximum load.

The mechanism responsible for ETB appears to be magnesium assisted sulfur segregation. The identification of this mechanism is based upon correlations between magnesium, sulfur and the occurrence of ETB. As a result of this realization, ferritic ductile iron compositions containing low sulfur and/or low magnesium levels have been formulated in accordance with the invention so as to be substantially immune to ETB.

The occurrence of ETB is studied through examination of a value defined as a "ductility ratio" which is the elevated temperature ductility measured at 425C (800F) divided by the ductility at room temperature. The ductility ratio separates ETB effects from other effects on ductility. Alloying and microstructures effect both room temperature ductility as well as elevated temperature ductility so as to leave the ductility ratio unchanged. However, ETB effects only elevated temperature ductility and thus dramatically changes the ductility ratio. Reliance on elevated temperature ductility alone as an indicator of ETB would provide a much weaker correlation due to the clouding or obfuscating effects of alloying and microstructure.

Most of the presently marketed ferritic ductile iron is susceptible to ETB and would therefore offer limited temperature capability. By eliminating ETB as taught by the invention, an improved alloy is obtained which has comparable elevated temperature fatigue resistance to plain carbon or low alloy steels.

It is therefore a primary object of the invention to provide a ferritic ductile iron composition which is rendered substantially immune to ETB by controlling and limiting the residual concentrations of magnesium and sulfur.

BRIEF DESCRIPTION OF THE DRAWINGS AND TABLES

Various other objects, features and attendant advantages of the present invention will be more fully appreciated as the same becomes better understood from the following detailed description when considered in connection with the accompanying tables and drawings wherein:

Table 1 is a listing of various ferritic ductile iron heat chemistries identifying each component in weight percent;.

Table 2 is a listing of ferritic ductile iron heat treatments and microstructures;

Table 3 is a listing of fracture characteristics of heats G and H;

Figure 1 is a fitted plotting of tensile area reduction of heats B, E, G and H as a function of temperature;

Figure 2 is a fitted plotting of the fracture strength of heats B, E, G and H as a function of temperature;

Figure 3 is a metallographic fracture sectioning of a tensile specimen taken from heat G identifying areas of intergranular fracture and shrinkage porosity (enlarged 200X) tested at 425C (800F), nital etch;

Figure 4 is a metallographic fracture sectioning of a tensile specimen taken from heat H (enlarged 200X) tested at 425C (800F), nital etch;

Figure 5 is a fitted plotting of a dependence of elevated temperature ductility of ferritic ductile iron on magnesium and sulfur content wherein an ETB immunity region is defined between the plot axes and the line $Mg + 4.5S = 0.07$;

Figure 6 is a fitted plotting of tensile area reduction as a function of strain rate and temperature of heats G and H;

Figure 7 depicts fracture stress as a function of strain rate and temperature for heats G and H.

Figure 8a is a view of the fracture surface of a tensile specimen of heat G identifying areas of intergranular fracture and shrinkage porosity (enlarged 200X) tested at 370C (700F), at a strain rate of 4.4×10^{-5} sec $^{-1}$;

Figure 8b is a view of the fracture surface of a tensile specimen of heat G identifying areas of intergranular fracture and shrinkage porosity (enlarged 1000X), tested at 370C (700F), at a strain rate of 4.4×10^{-5} sec $^{-1}$;

Figure 9a is a view of the fracture surface of a tensile specimen of heat H (enlarged 200X), tested at 370C (700F), at a strain rate of 4.4×10^{-5} sec $^{-1}$;

Figure 9b is a view of the fracture surface of a tensile specimen of heat H (enlarged 1000X), tested at 370C (700F), at a strain rate of 4.4×10^{-5} sec $^{-1}$;

Figure 10 is a transmission electron microscope relief replica fractograph of the intergranular fracture area on a specimen of heat G (enlarged 10,000X);

Figure 11 is a transmission electron microscope relief replica fractograph of the shrinkage area on a specimen of heat G (enlarged 10,000X);

Figure 12 depicts the intergranular fracture area on a specimen of heat E identifying areas of intergranular fracture and shrinkage porosity (enlarged 500X), pre-strained at 425C (800F);

Figure 13 shows the low cycle fatigue behavior of ferritic ductile iron tested at 425C (800F);

Figure 14a depicts a fracture surface of a specimen of heat B (enlarged 75X), low cycle fatigue tested at 425C (800F);

Figure 14b depicts a fracture surface of a specimen of heat B (enlarged 500X), low cycle fatigue tested at 425C (800F);

Figure 15a depicts the fracture surface of a specimen of heat H (enlarged 75X), low cycle fatigue tested at 425C (800F);

Figure 15b depicts the fracture surface of a specimen of heat H (enlarged 500X), low cycle fatigue tested at 425C (800F);

Figure 16 shows the effect of strain rate on elevated temperature ductility of ferritic ductile iron; and

Figure 17 is a comparison of low cycle fatigue properties of heats H, I, J and K to cast steel A216WCC and plate steel A516-Gr55 (transverse orientation) at 425C (800F).

DETAILED DESCRIPTION OF THE PREFERRED EMBODIMENT

In order to better understand the phenomenon of elevated temperature brittleness in ferritic ductile iron, an in-depth investigation was conducted to study the effects of chemical composition, strain rate and temperature on ETB. Twenty-six different material compositions representing a wide range of ferritic ductile iron chemistry were selected for study. The chemical composition of each heat is set forth in Table 1 and a description of each heat in terms of heat treatment and microstructure is set forth in Table 2.

The general mechanical behavior of ferritic ductile iron in the ETB regime was studied with the aid of tensile and low cycle fatigue testing. The tensile tests were in four series, the first series involving air testing 6.35 mm diameter test specimens from room temperature to 650C (1200F) using standard ASTM practice. Primary emphasis was on heats B, E, G and H. The strain rate in these tests was 8.3×10^{-5} sec $^{-1}$, up to yielding and than 8.3×10^{-4} sec $^{-1}$ to fracture.

Microscopic examination of failed tensile and fatigue test specimens was performed using longitudinal sectioning, scanning electron microscopy, relief replica transmission electron microscopy and energy dispersive X-ray analysis.

Figure 1 shows the reduction in area from the first series of tensile tests as a function of temperature for heats B, E, G and H. The ETB regime is sharply delineated at 425C (800F). It is important to note that heat H appears substantially unaffected by ETB and clearly shows less brittleness than the other heats.

The ETB regime is less clearly seen in the fracture stress data plotted in Figure 2. Even so, heat H, a preferred heat, displays a higher fracture stress although all heats show a rapid decline in fracture stress with increasing temperature. Metallographic sectioning of 425C (800F) tested specimens of heats G and H indicate the presence of intergranular fracture in heat G, as shown in Figure 3, while none was found in heat H, as shown in Figure 4.

From the room temperature and 425C (800F) tensile testing of the entire group of heats listed in Table 1, the ratio of ETB minimum area reduction to room temperature area reduction, expressed as a ductility ratio "DR" is seen to correlate with the combination of magnesium (Mg) and sulfur (S) content of each heat. This correlation is shown in Figure 5. The DR value clearly separates ETB effects from variations in mechanical properties due to alloying or microstructure. A ductility ratio of near unity implies behavior to heat H while a ratio near one-fourth implies behavior similar to heat G. Clearly, a poor ductility ratio is associable with elevated Mg and S content. By maintaining the parameter (Mg + 4.5S) below .07, ETB is avoided. This represents a triangular region as shown in the left side of Figure 5. The fact that ETB behavior is well defined by the residual Mg and S content strongly suggests a major role of these two elements.

Figure 5 includes data from heats containing degenerate graphite (ASTM Type IV). Such structures usually reflect Mg "fade" or an insufficient Mg addition, and may be unacceptable in spite of their immunity to ETB.

The second series of constant displacement tensile tests were performed on a Gleeble 1500 test machine. Data from these tests provides evidence of the effect of strain rate on ETB. Figure 6 shows area reduction data for heats G and H. The relative superiority in ductility and lower temperature minimum of heat H is again clear. Moreover, it is clear that the temperature of minimum area reduction is 130C (235F) higher for the higher strain rate. Additionally, the ETB temperature range (the range over which the area reduction is reduced) is greater for the higher strain rate. The effect of strain rate on fracture stress is shown in Figure 7.

The difference in embrittlement observed between heats G and H (among others) may be related, by fractography, to the degree of intergranular fracture as shown in Figures 8a and 8b. The pronounced embrittlement of heat G is associated with extensive intergranular fracture and the presence of shrinkage porosity within the intergranular fracture region. Figures 9a and 9b show the classical dimpled rupture behavior that dominates the less brittle heat H.

A quantitative description of the extent of intergranular fracture is given in Table 3 and noted in Figure 6 for many of the Gleeble machine tested specimens. A representative transmission electron microscope relief fractograph of an intergranular surface tensile tested at 425C (800F) is shown in Figure 10. Likewise, transmission electron microscope fractography confirms that porosity is the result of shrinkage during solidification, as shown in Figure 11.

A third series of two-stage interrupted tensile tests provides a clear delineation of intergranular fracture areas and reveals that such fracture initiates at shrinkage pores. These tests involved first pre-loading the test bar at 425C (800F) using standard ASTM tensile test procedures and then interrupting the test prior to reaching maximum load. The pre-loaded bars were then tested at room temperature to reveal fracture initiation behavior. Figure 12 shows a scanning electron microscope fractograph from one of these interrupted tensile tests. It is clear from these tests that fracture initiates at shrinkage pores in the ETB temperature range.

Strain controlled low cycle fatigue test results are presented in Figure 13. A clear difference in fatigue resistance is evident. Those heats exhibiting superior low cycle fatigue resistance also have reduced elevated temperature brittleness response. These results correlate with the Mg and S correlation (DR ratio) discussed above.

A scanning electron microscope fractographic examination of a heat B low cycle fatigue specimen identifies intergranular fracture and associated shrinkage porosity as shown in Figures 14a and 14b. Examination of heat H shows only transgranular fracture in Figures 15a and 15b.

The above test results provide evidence as to the ETB fracture mechanism. From the observation that intergranular fracture initiates from the shrinkage pores, the fracture mechanism can be related to the last liquid to solidify or to segregation. A dependence of such fracture upon Mg and S is also shown. Since Mg is relatively insoluble in iron, segregation to grain boundaries should occur in the last liquid to solidify. Mg is usually combined and, since it is added to the melt to scavenge impurities such as sulfur, some minor amount of magnesium sulfide (MgS) should be present in the melt during solidification. The amount of MgS residing in the grain boundaries would depend on many factors including melt chemistry, magnesium additions and time. The time factor would explain the benefit of magnesium "fade" which results in ASTM Type IV graphite and improved fatigue resistance. Despite these variables, the residual amounts of magnesium and sulfur are directly relatable to the occurrence or immunity to ETB.

Once formed, MgS is unstable at temperature above room temperature and, with time, decomposes into magnesium oxide (MgO) and free sulfur upon cooling from solidification or during heat treatment. In bulk form, sulfur has a boiling point of 455C (855F), which is coincidentally close to the temperatures observed for ETB. All of the above suggest that ETB is the result of magnesium assisted sulfur segregation with sulfur as the embrittler and magnesium as the transport mechanism. This appears to explain the interrelation or synergy between magnesium and sulfur in which lower sulfur levels allow for higher magnesium levels before observing ETB.

The strain rate effect can be seen more clearly in Figure 16 which shows a plot of the temperature of minimum area reduction versus strain rate for heat G. Onset and recovery temperatures can be identified from the temperatures at which heats G and H show comparable area reduction above and below the minimum. From Figure 16 a clearer understanding of the strain rate effect on ETB affected heats is obtained. This behavior has similarities to metal induced embrittlement.

The temperature for onset of ETB can be related to the mobility of sulfur, and as such should be diffusion controlled. That is, that in order for intergranular fracture to contribute significantly to the overall fracture process, sulfur must be mobile enough to keep pace with the damage rate. At low temperatures and/or high strain rates, sulfur is presumably not mobile enough to keep pace with the damage rate and only ductile fracture occurs because of insufficient time for the movement of sulfur.

Recovery may occur from the possibility that free sulfur oxidizes and is prevented from causing further embrittlement. This process would also be diffusion controlled and would be predominant at the specimen surface. That is to say that at higher temperatures and longer times (slow strain rates), oxygen may have sufficient mobility to reach intergranular crack fronts and prevent further crack advance.

Whatever the mechanism for ETB may be, the Mg-S correlation indicates that low sulfur is highly important. The reduction of sulfur levels leads to wider ranges of acceptable Mg levels and to a lower propensity for degenerated graphite.

It can be appreciated that the present invention is based on the identification of a number of heats of ferritic ductile iron which do not exhibit ETB. Of particular interest is heat H which is substantially immune to ETB. A comparison of the fatigue properties of some of these heats with two commonly used steels is shown in Figure 17. The ductile iron heats are comparable in fatigue capability to these steels.

Based on the test results discussed above, the following observations can be made regarding the elevated temperature brittleness of ferritic ductile iron:

1) Elevated temperature brittleness acts to reduce tensile strength, tensile ductility and fatigue resistance.

2) ETB is observed in an elevated temperature range which is strain rate dependent. For a strain rate of 4.4×10^{-5} sec $^{-1}$, the temperature range is 310C (590F) to 490C (914F), while for a strain rate of 2.0×10^{-2} sec $^{-1}$, the range is 370C (700F) to 760C (1400F).

3) The temperature at which tensile area reduction is minimum moves to higher temperatures with increasing strain rate. For a strain rate of 4.4×10^{-5} sec $^{-1}$, the area reduction minimum occurs at 400C (725F), while for a strain rate of 2.0×10^{-2} sec $^{-1}$, the minimum occurs at 530C (986F).

4) Onset and recovery occurs similar to metal induced embrittlement.

5) Intergranular fracture is associated with reduced tensile ductility and at the ductility minimum can account for up to 35 percent of the fracture surface.

6) Intergranular fracture initiates at shrinkage pores.

7) The ductility ratio, which is the ratio of area reduction at the ductility minimum temperature (taken as 800F RA) to that at room temperature, correlates with magnesium and sulfur levels. Low magnesium and/or low sulfur levels lead to relative immunity to ETB. A value of DR near one-fourth indicates full ETB while a value near unity indicates relative immunity to ETB.

8) ETB appears to be the result of magnesium assisted sulfur segregation. The residual percent by weight level of sulfur and magnesium combined into the parameter (Mg + 4.5S) should be maintained below 0.070 percent by weight in order to avoid ETB.

9) Low cycle fatigue life is severely affected by ETB in a similar manner as tensile ductility.

Obviously, numerous modifications and variations of the present invention are possible in light of the above teachings. It is therefore to be understood that within the scope of the appended claims, the invention may be practiced otherwise than as specifically described herein.

Table 1

Ferritic Ductile Iron
Heat Chemistries
(Wt. Pct.)

Heat	C	Si	Ni	Mo	Mn	P	Mg	S	Ti	V	Al	Cu	Cr
A	3.60	2.29	0.99	0.05	0.22	.015	.052	.009	.011		.020	.045	.089
B	3.60	2.20	0.38	0.74	0.23	.018	.048	.016	.015		.039	.035	.063
C	3.38	3.07	0.26	0.47	0.10	.020	.057	.007					
D	3.69	2.37	0.05	0.61	0.22	.017	.061	.018	.025	.008	.056	.031	.063
E	3.70	2.78	0.15	0.57	0.19	.016	.048	.016	.029		.052	.051	.064
F	3.50	2.38	0.75	0.50	0.10	.016	.038	.008	.024	.024	.039	.044	.083
G	3.43	2.21	1.23	0.40	0.09	.017	.053	.009	.024	.024	.029	.048	.075
H	3.55	2.63	0.13	0.61	0.09	.017	.023	.008	.025	.022	.059	.045	.071
I	3.61	2.72	0.07	0.59	0.07	.019	.029	.005	.020	.030		.010	.030
J	3.46	3.00	0.73	0.80	0.09	.022	.025	.008	.033	.033	.115	.019	.061
K	3.55	3.29	0.59	0.95	0.07	.020	.026	.005	.021	.040		.010	.050
L	3.43	3.08	0.60	1.35	0.07	.024	.017	.005					
M	3.55	2.60	0.96		0.17	.007	.033	.007			.007	.022	.080
N	3.35	2.53	0.13	0.03	0.05	.020	.036	.009	.014	.026	.034	.043	.055
O	3.54	2.86	0.88	0.57	0.02	.018	.025	.009			.031		.056
P	3.38	2.70	1.51	0.66	0.02	.014	.035	.005	.025	.041	.020	.026	.051
Q	3.45	2.72	0.55	0.68	0.05	.018	.022	.008	.024	.040		.010	.090
R	3.60	3.30	0.49	0.01	0.02	.005	.022	.007	.027	.010		.010	.010
S	3.47	3.00	0.50	0.64	0.02	.017	.028	.008	.024	.010		.010	.010
T	3.60	2.71	0.48	0.01	0.02	.008	.029	.009	.034	.010		.010	.120
U	3.64	2.70	0.03	0.00	0.26	.030	.047	.005	.008	.003	.017		.032
V	3.56	2.60	0.03	0.00	0.24	.024	.050	.004	.004	.002	.015		.028
W	3.66	2.52	0.03	0.00	0.24	.022	.052	.004	.008	.007	.018		.027
X	3.66	2.50	0.04	0.01	0.25	.028	.061	.003	.016	.011	.020		.036
Y	3.64	2.16			0.28	.020	.016	.006					
Z	3.49	2.68			0.38	.020	.018	.008					

Table 2

Ferritic Ductile Iron
Heat Microstructure

Heat	Heat(1) Treatment	ASTM Graphite % Type I & II / % Type IV	% Pearlite
A	FA	99/1	5
B	FA	99/1	7
C	FA	99/1	7
D	FA	99/1	5
E	FA	99/1	5
F	SCA	99/1	10
G	SCA	99/1	7
H	SCA	99/1	3
I	FA	99/1	3
J	SR	99/1	5
K	SCA	99/1	5
L	SCA	30/70	5
M	SCA	99/1	5
N	SCA	99/1	3
O	FA	10/90	7
P	FA	99/1	5
Q	SCA	50/50	3
R	SCA	99/1	3
S	SCA	99/1	3
T	SCA	99/1	5
U	SR	99/1	5
V	SR	99/1	3
W	SR	99/1	7
X	SR	99/1	3
Y	SCA	20/80	3
Z	SCA	10/90	3

(1) SR - As-cast with 595C stress-relief anneal
SCA - Sub-critical anneal only (720C)
FA - Full anneal (critical anneal at 900C and sub-critical anneal at 720C)

TABLE 3

FRACTURE CHARACTERISTICS

OF HEATS G AND H

HEAT	SPEC NO.	STRAIN RATE -1 SEC.	TEMP (C)	TEMP (F)	% INTERG. FRAC.	% SHRINK POROS.
G	8	4.4×10^{-5}	370	700	22.7	3.0
	3	"	425	800	36.5	3.8
	13	2.0×10^{-2}	425	800	0.0	5.9
	17	"	480	900	15.9	3.5
	18	"	540	1000	35.4	6.2
	15	"	595	1100	17.6	5.1
H	5	4.4×10^{-5}	425	800	<1.0	2.3
	10	2.0×10^{-5}	540	900	<1.0	1.1

Claims

1. A ferritic ductile iron composition having a substantial resistance to elevated temperature brittleness, said iron comprising a residual quantity of sulfur in a weight percentage of no greater than 0.015.

2. The iron composition of claim 1, further comprising a residual quantity of magnesium in a weight percentage of no greater than 0.070.

3. The iron composition of claim 1, further comprising the combination of residual quantities of magnesium and sulfur into the parameter (Mg + 4.5S) in weight percentage of no greater than 0.070.

4. The iron composition of claim 1, wherein said iron composition is a sub-critical annealed or full anneal iron.

5. The iron composition of claim 1, further comprising a microstructure including a quantity of pearlite in a range of 3% to 10% by weight.

6. The iron composition of claim 1, further comprising graphite.

7. The iron composition of claim 6 wherein said graphite comprises approximately 10 to 99 percent by volume ASTM Type I or Type II graphite.

8. The iron composition of claim 6 wherein said graphite comprises approximately one to 90 percent by weight ASTM Type IV graphite.

9. The iron composition of claim 4, wherein said full annealed iron is critically annealed at a temperature of approximately 702C and sub-critically annealed at approximately 595C.

10. The iron composition of claim 5, wherein said quantity of pearlite is present in a quantity of approximately 3% to 5% by weight.

11. The alloy of claim 1 wherein said alloy comprises a shrink porosity within the range of approximately 1.1 to 6.2%.

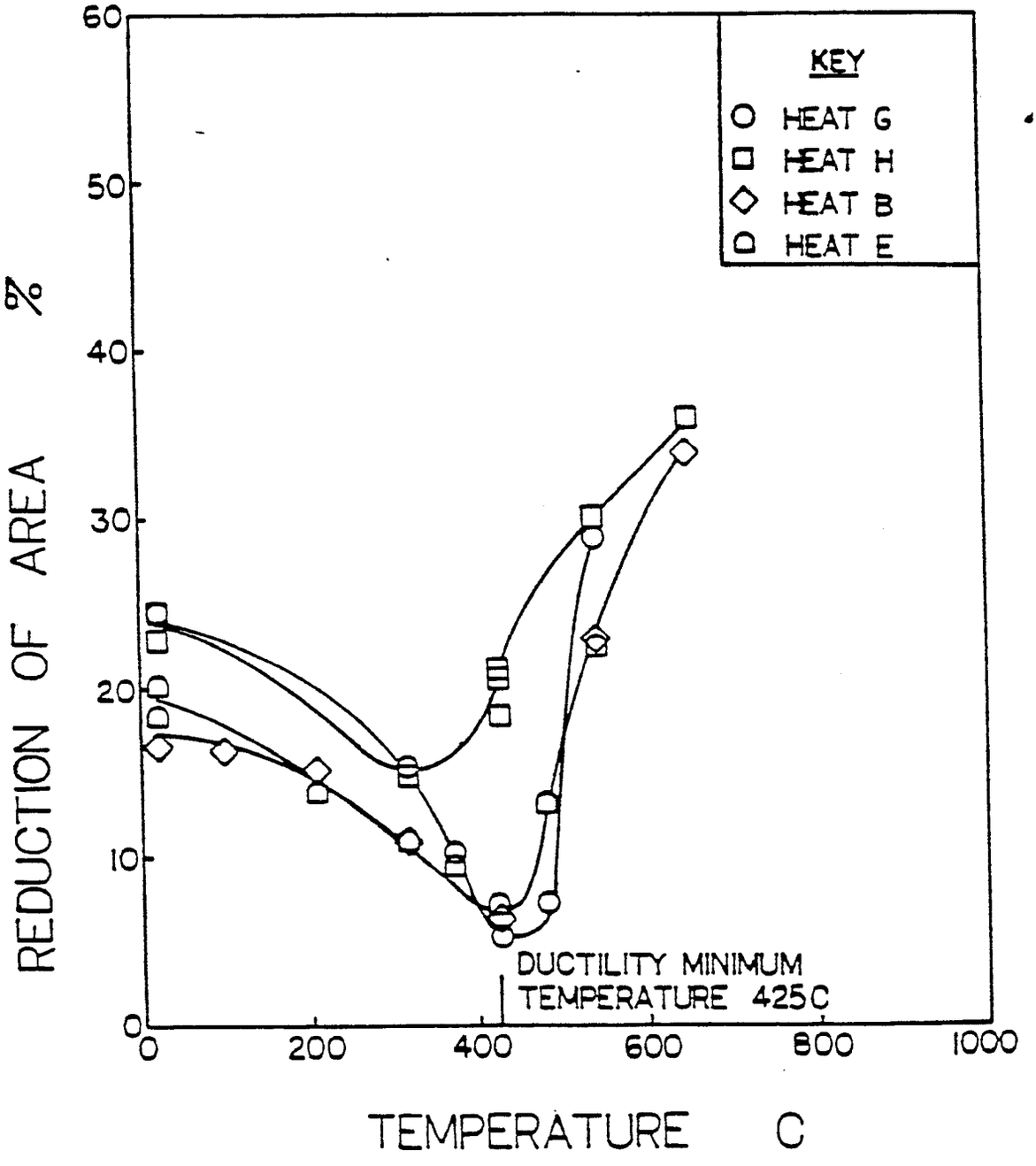

Figure 1. Tensile Area Reduction of Heats B, E, G and H as a Function of Temperature

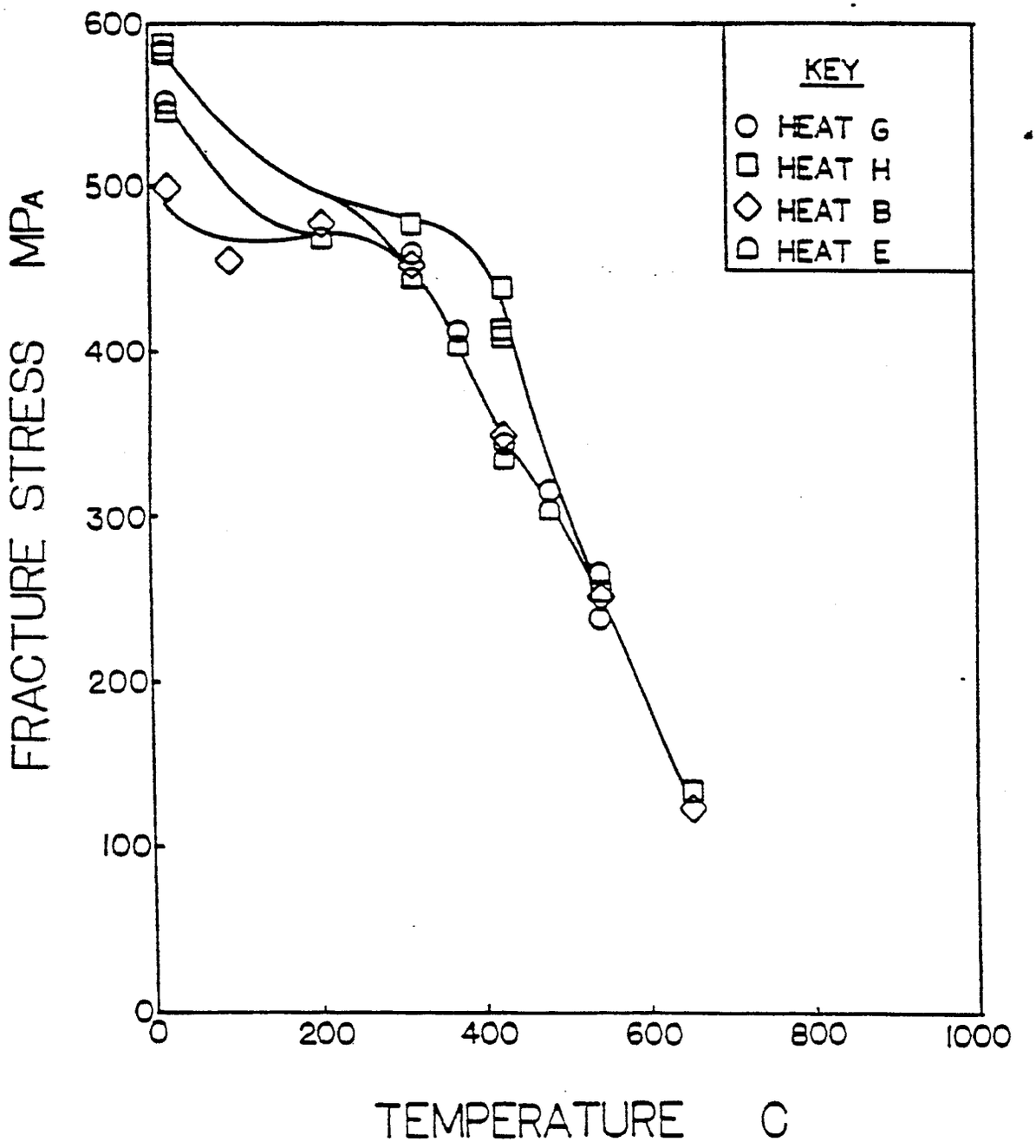

Figure 2. Fracture Strength of Heats B, E, G and H as a Function of Temperature

Figure 3. Fracture of Tensile Specimen G4 Tested at 425C (800F) at 200X, Nital Etch

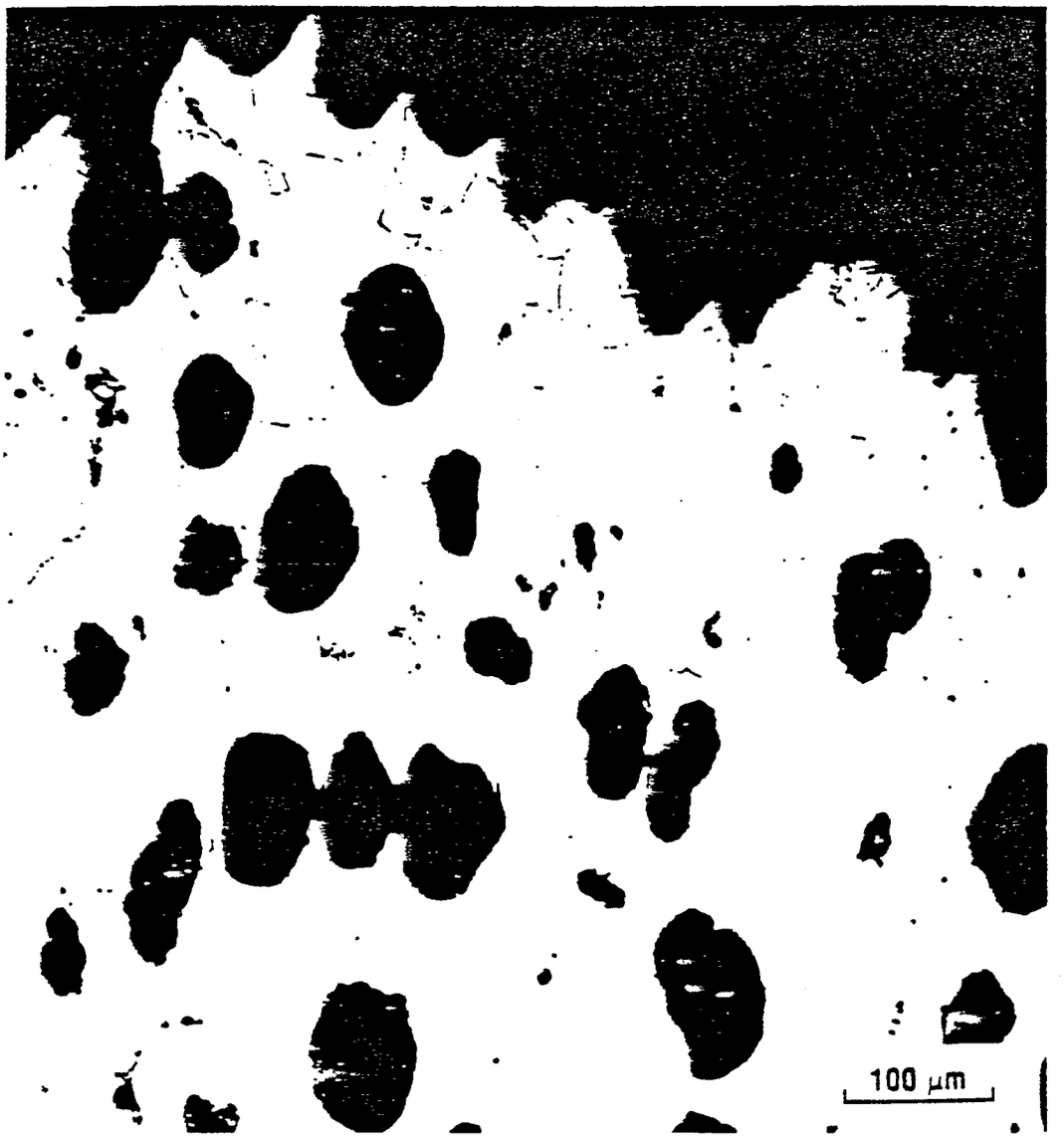

Figure 4. Fracture of Tensile Specimen H4 Tested at 425C (800F) at 200X, Nital Etch

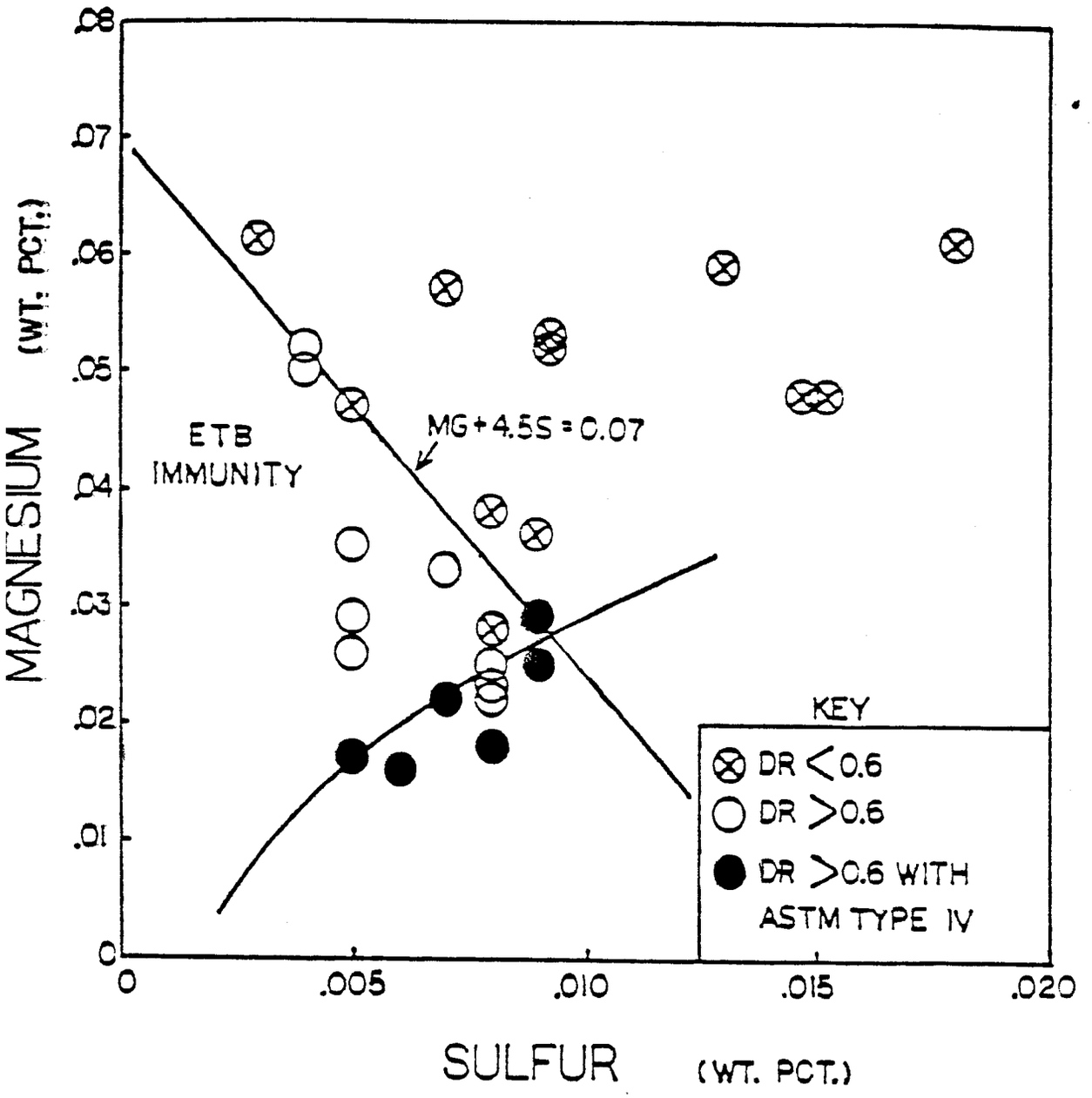

Figure 5. Dependence of Elevated Temperature Ductility of Ferritic Ductile Iron on Magnesium and Sulfur

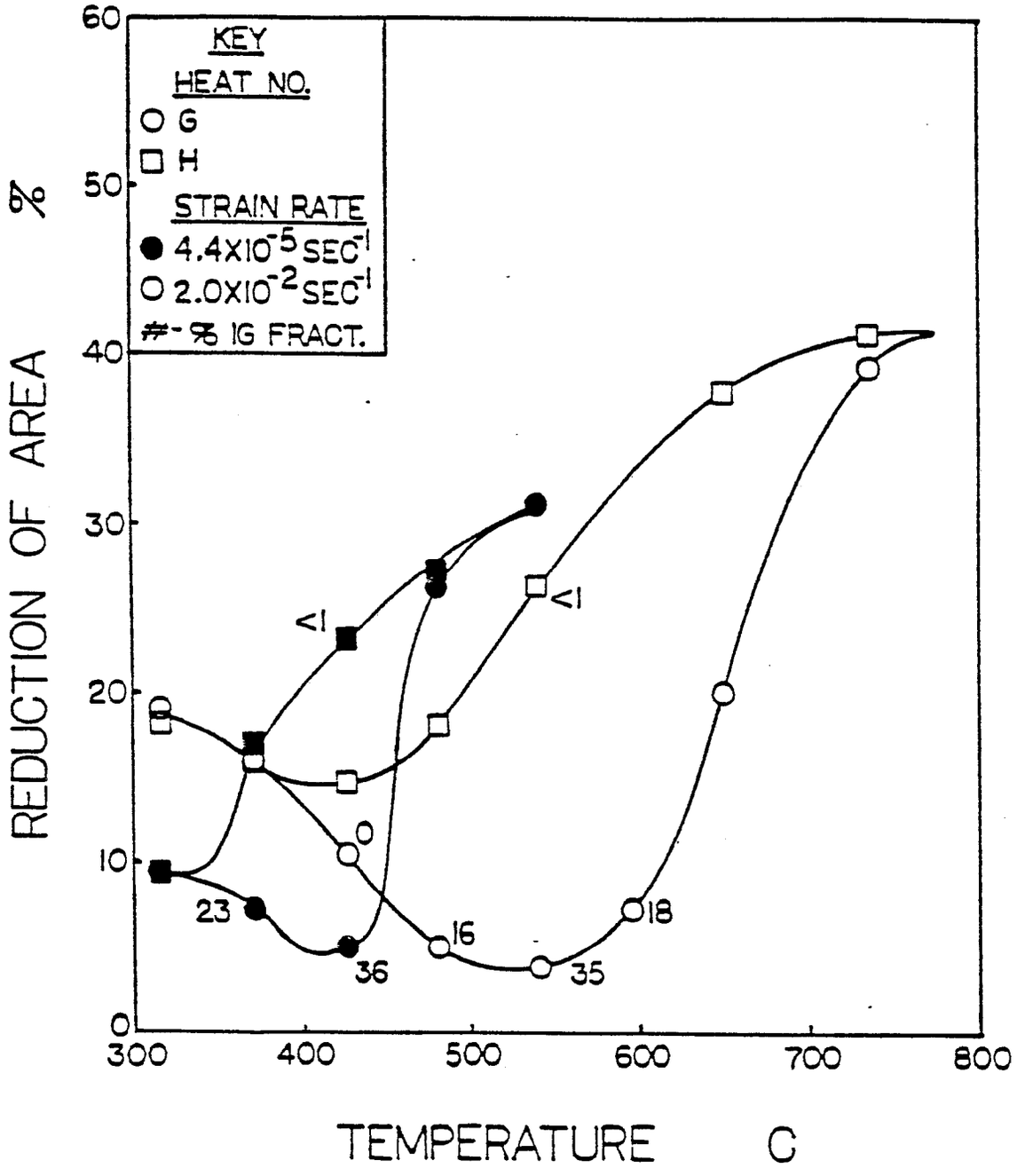

Figure 6. Tensile Area Reduction as a Function of Strain Rate and Temperature of Heats G and H

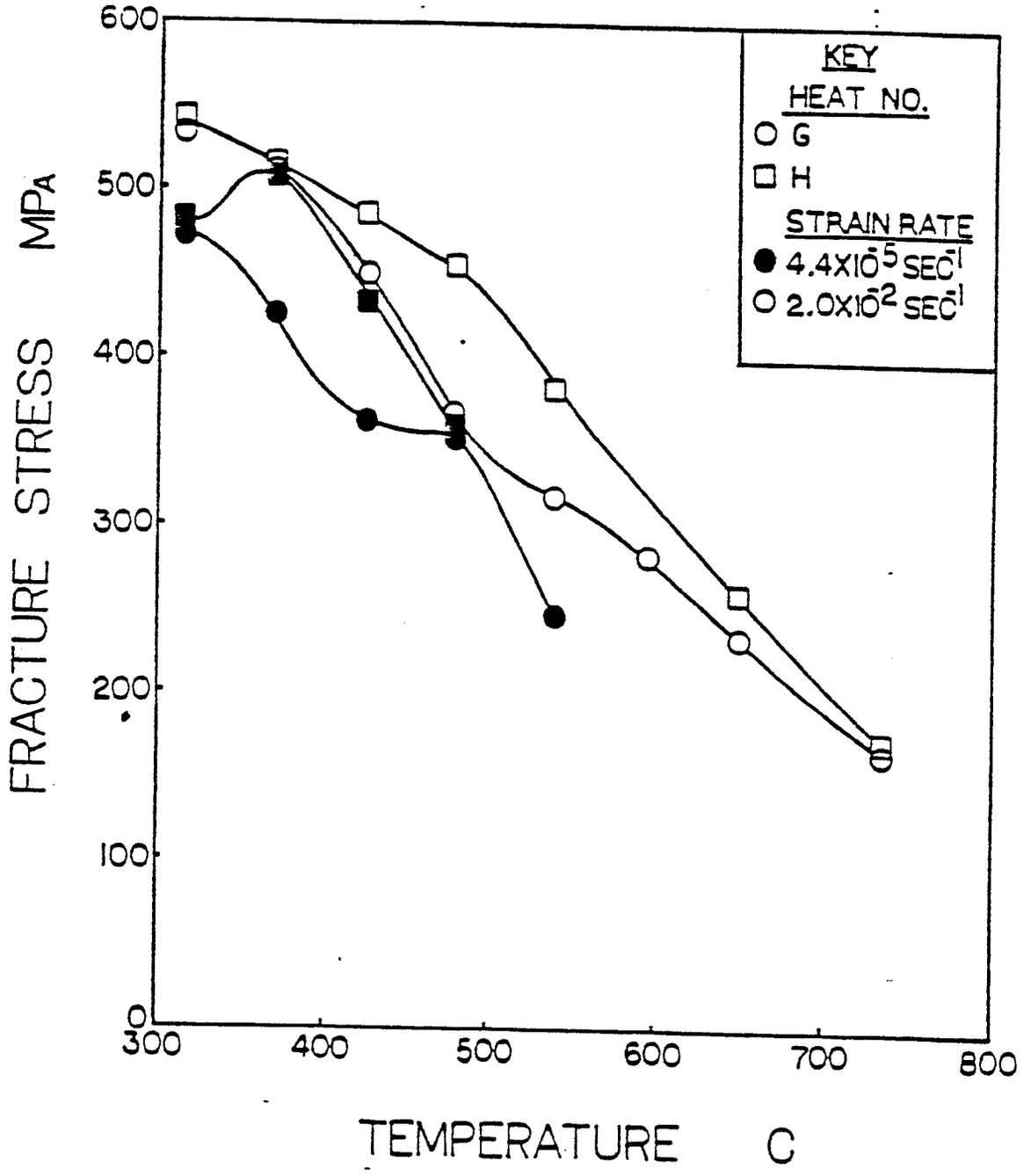

Figure 7. Fracture Stress as a Function of Strain Rate and Temperature for Heats G and H

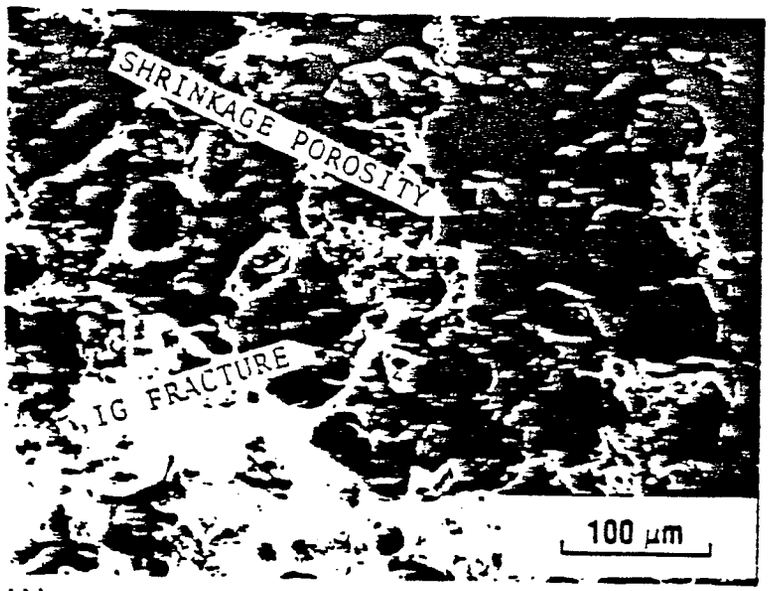

(A)

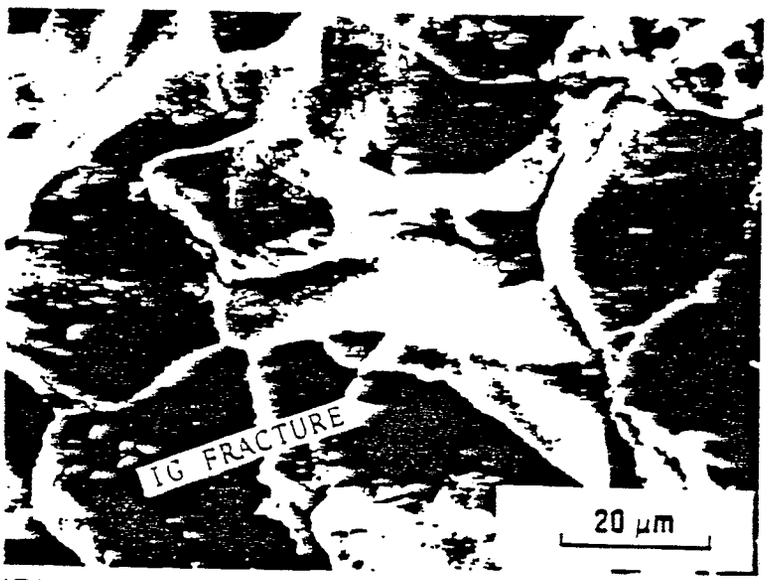

(B)

Figure 8. Fracture Surface of Tensile Specimen G8 Tested at 370C (700F) at a Strain Rate of 4.4×10^{-5} sec^{-1} at a) 200X and b) 1000X

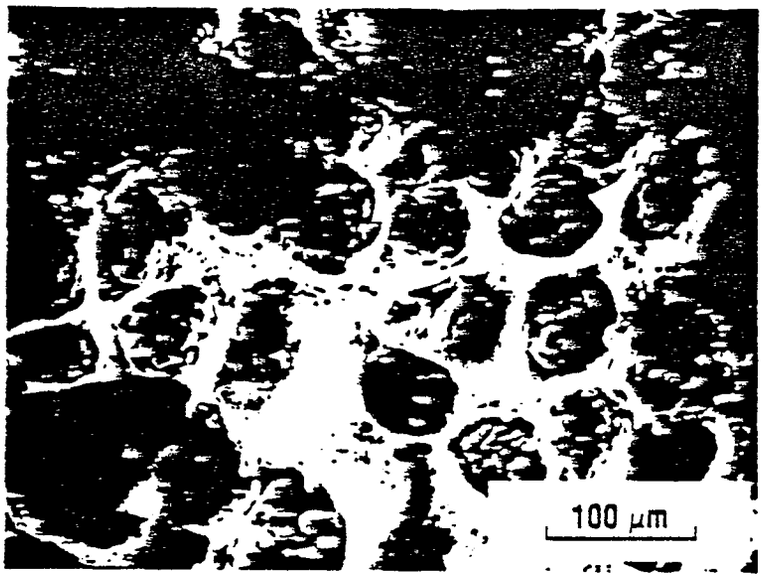

(A)

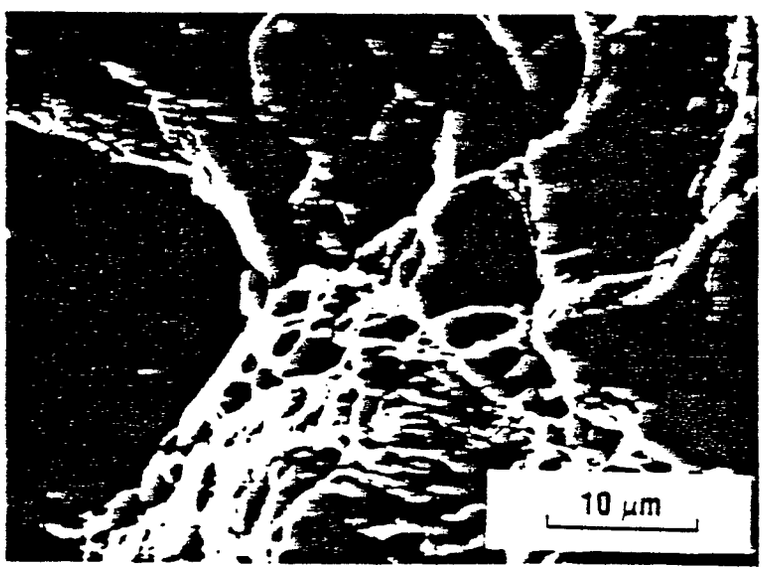

(B)

Figure 9. Fracture Surface of Tensile Specimen H2 Tested at 370C (700F) at a Strain Rate of 4.4×10^{-5} sec^{-1} at a) 200X and b) 2000X

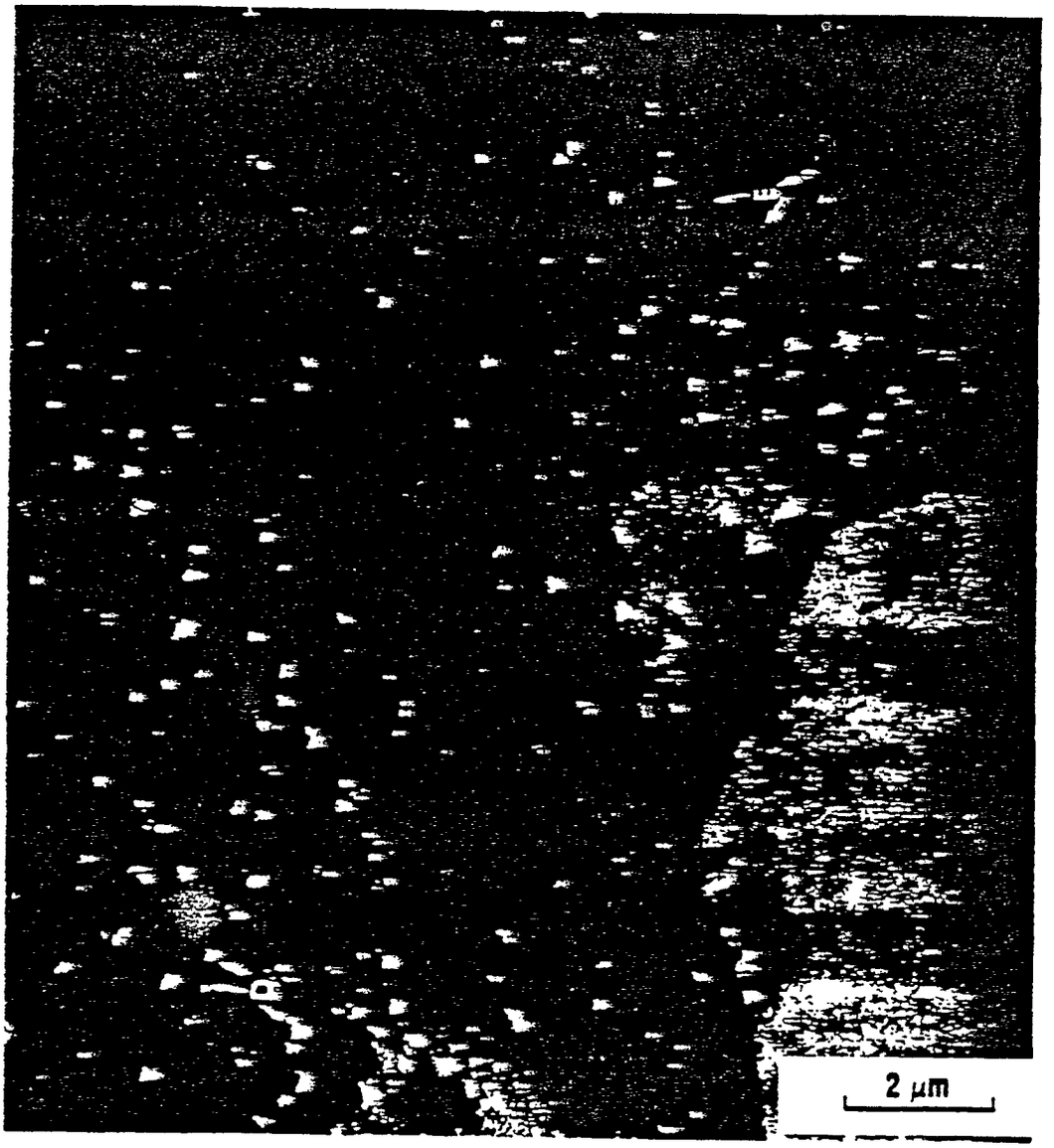

Figure 10. TEM Relief Replica of Intergranular Fracture Area on Specimen G3 at 10 KX

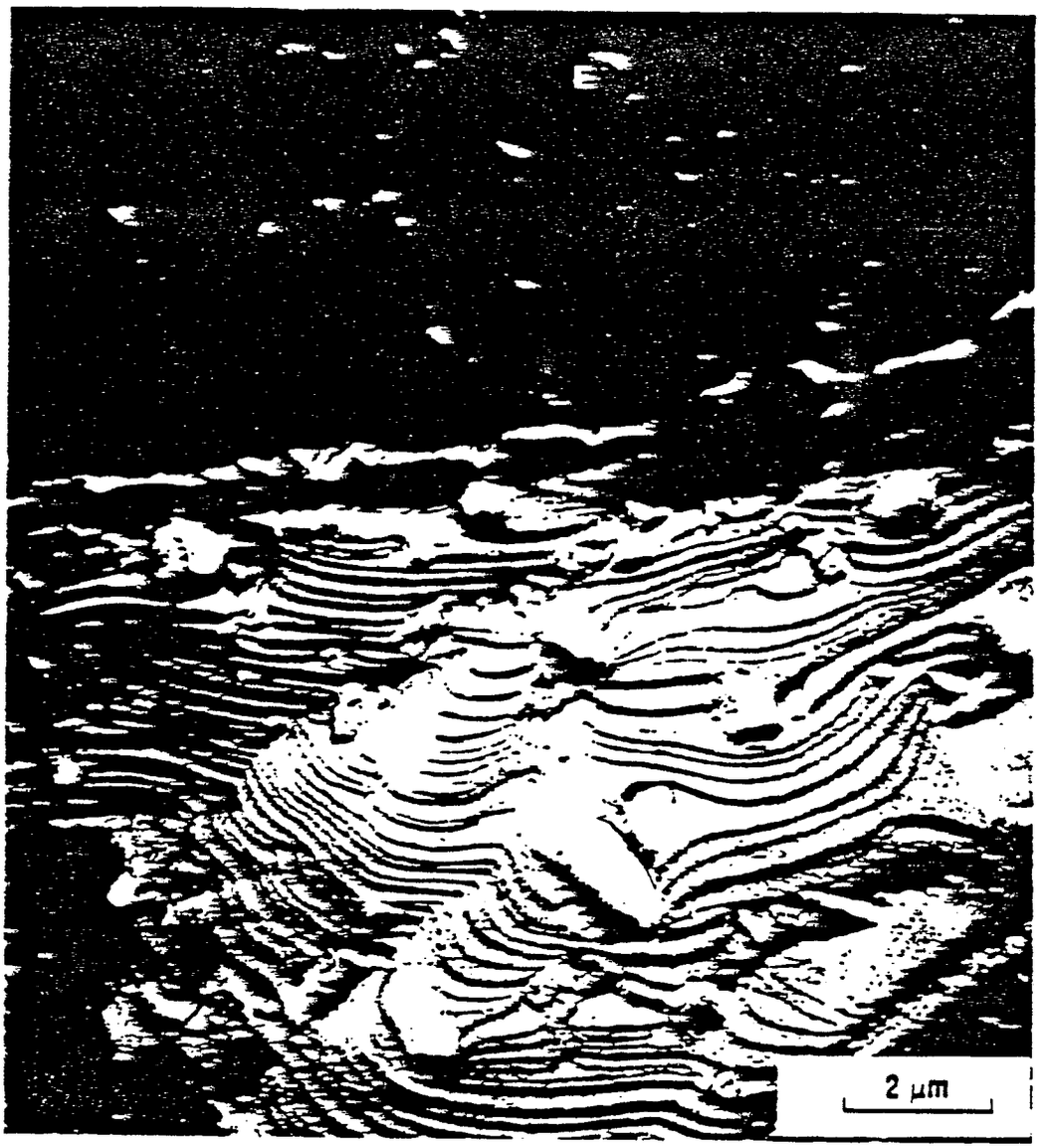

Figure 11. TEM Relief Replica of Shrinkage Area on Specimen G3 at 10 KX

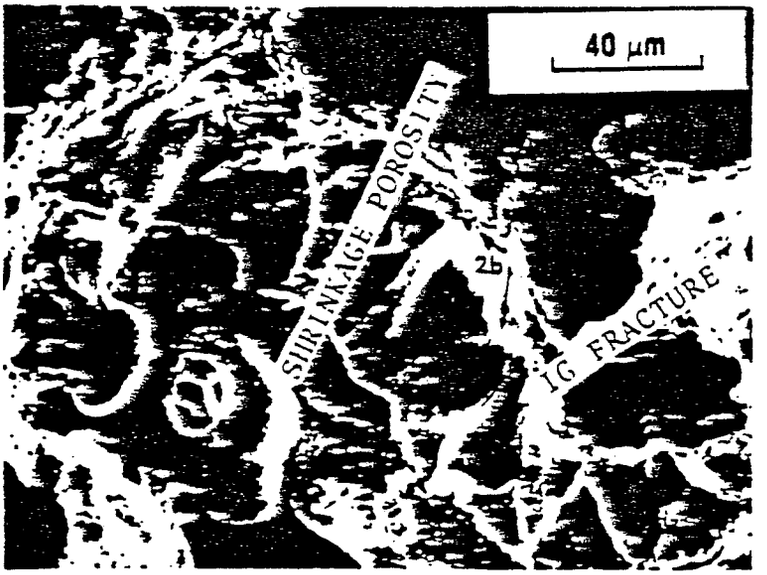

Figure 12. Intergranular Fracture Area on Specimen 9 of Heat E Pre-strained at 425C (800F) at 500X

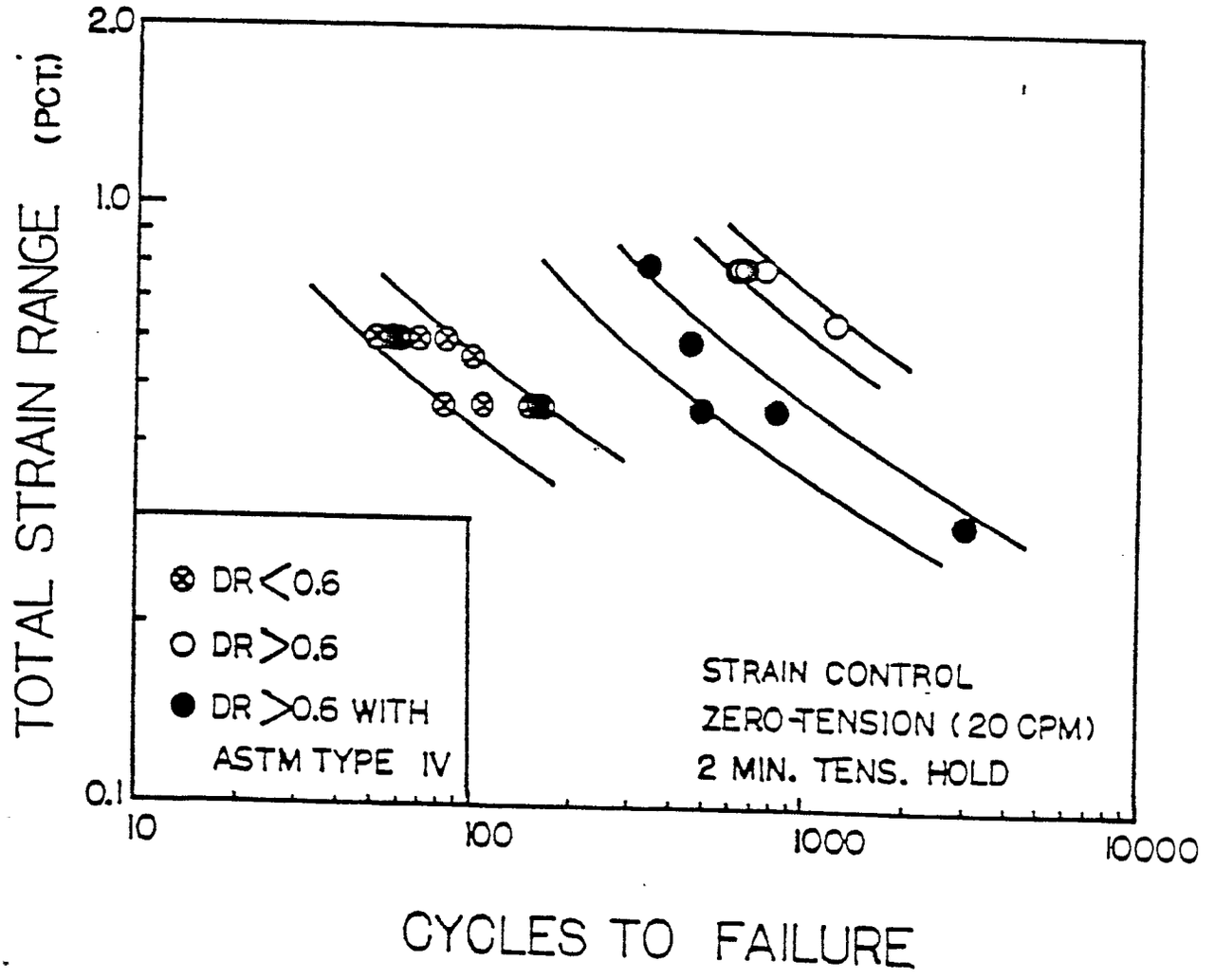

Figure 13. Low Cycle Fatigue Behavior of Ferritic Ductile Iron Tested at 425C (800F)

(A)

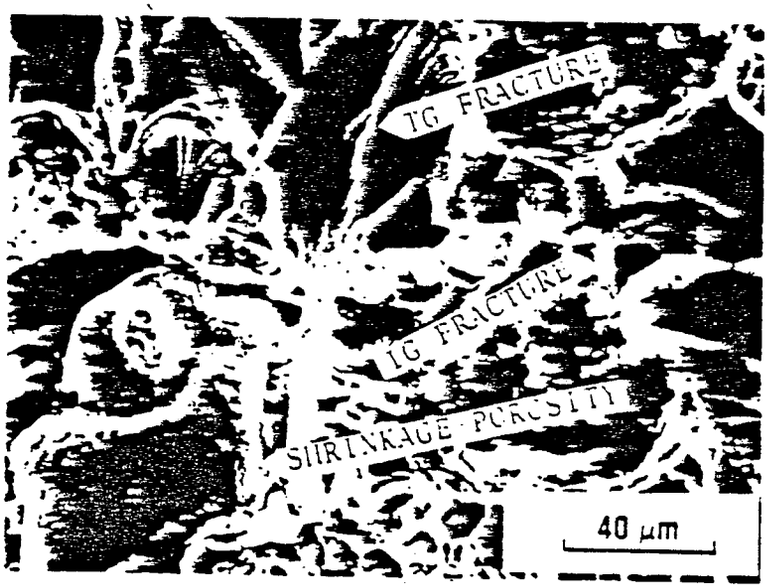

(B)

Figure 14. Fracture Surface of Specimen B1 Low Cycle Fatigue Tested at 425C (800F) at a) 75X and b) 500X

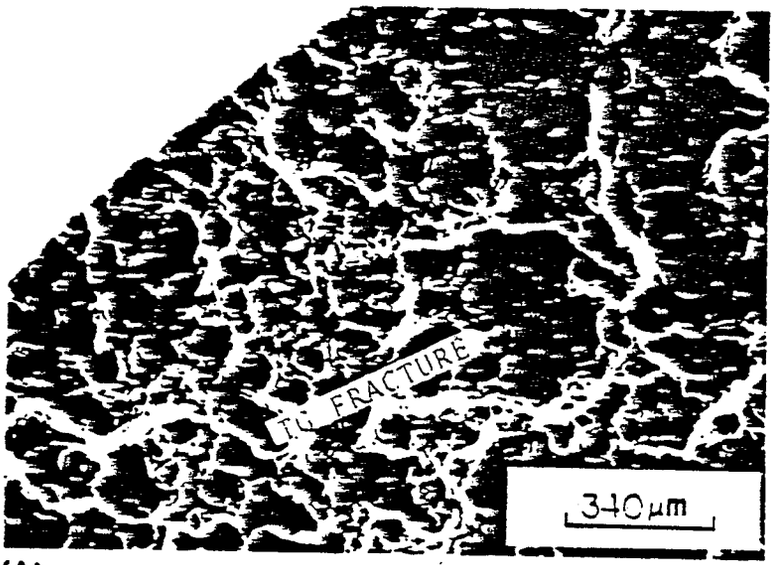

(A)

(B)

Figure 15. Fracture Surface of Specimen H1 Low Cycle Fatigue Tested at 425C (800F) at a) 75X and b) 500X

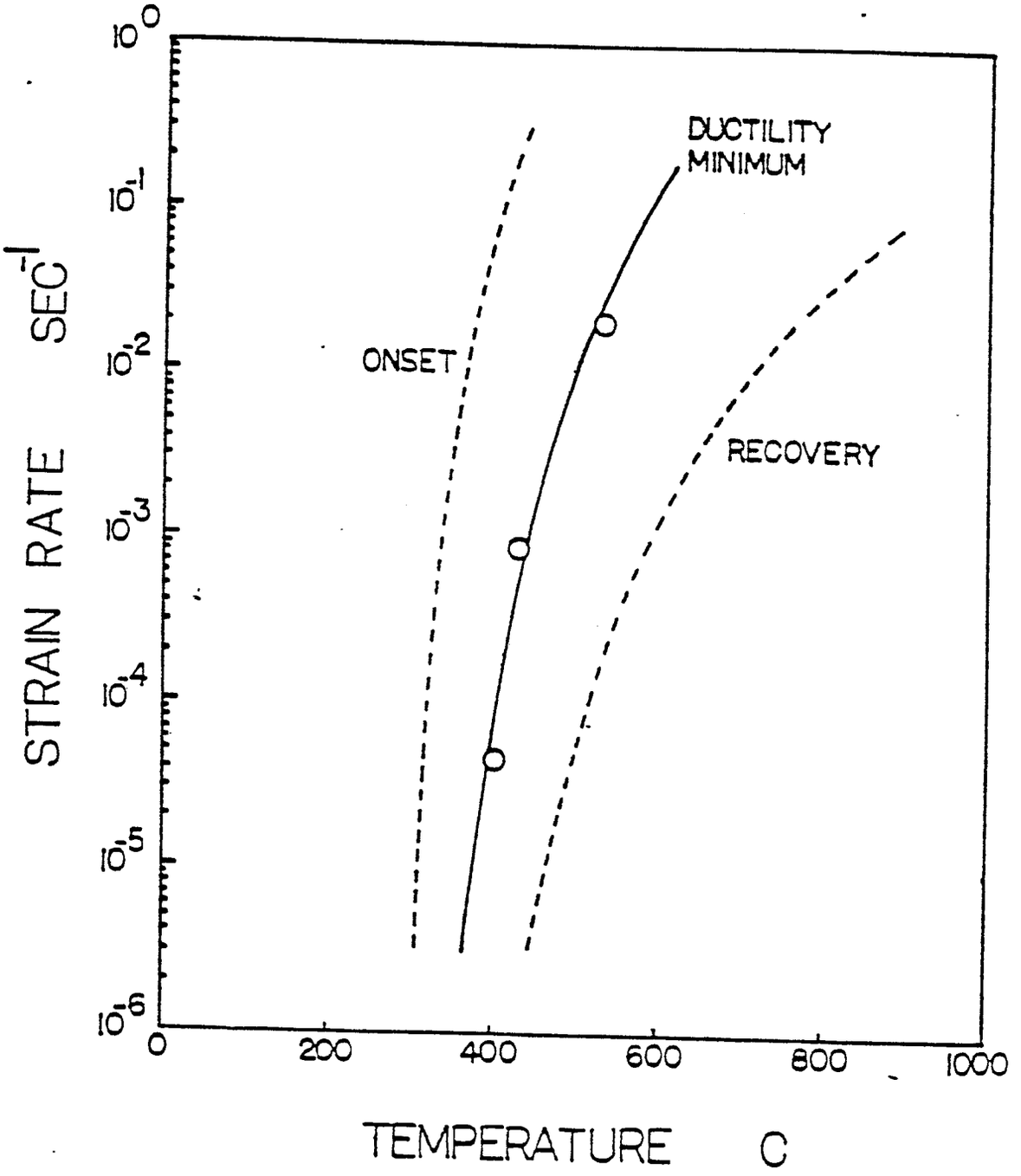

Figure 16. Effect of Strain Rate on Elevated Temperature Ductility of Ferritic Ductile Iron

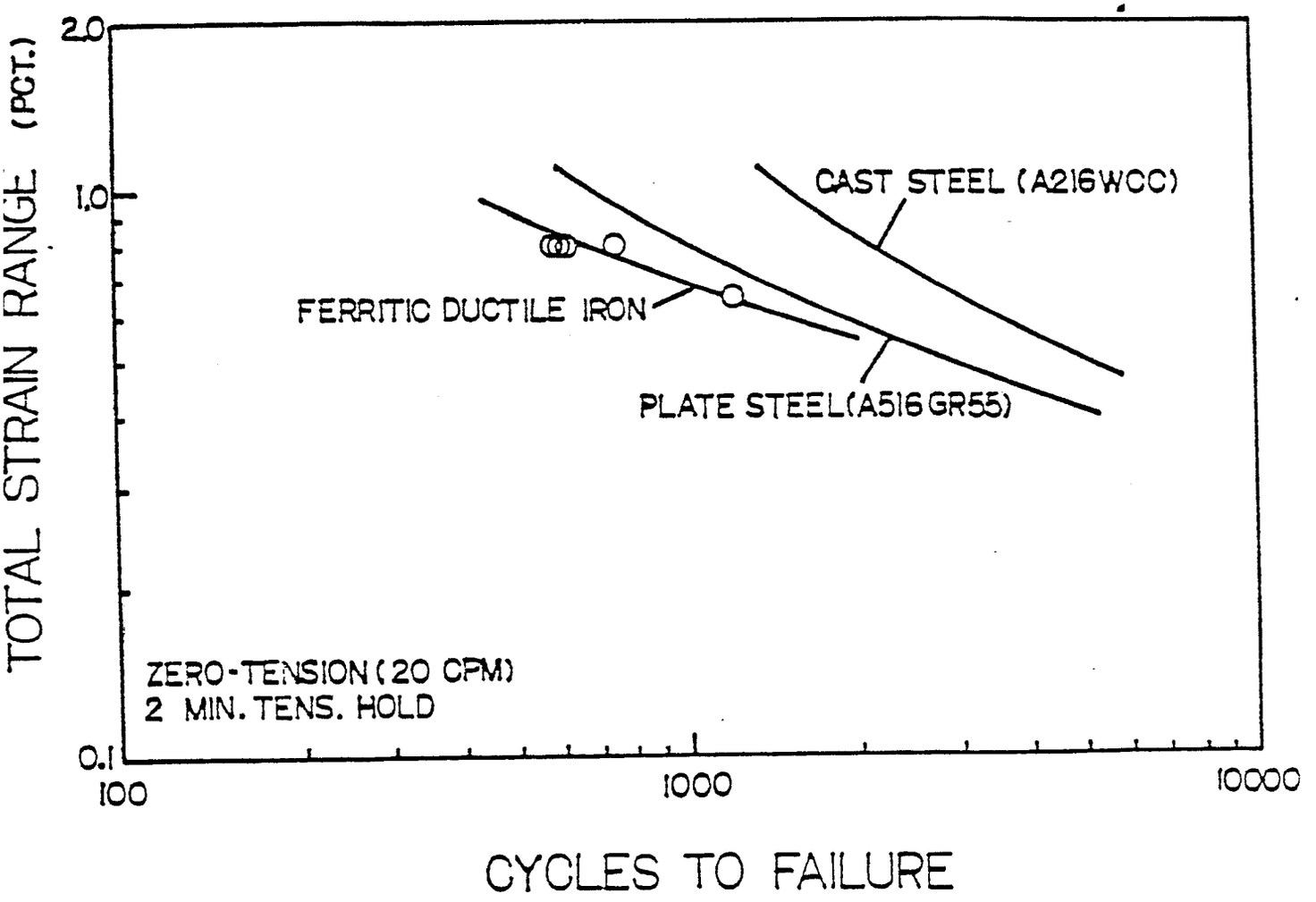

Figure 17. Comparison of Low Cycle Fatigue Properties of Heats H, I, J and K to Cast Steel A216WCC and Plate Steel A516-Gr55 (transverse orientation) at 425C (800F)